Preliminary performance assessment from towing tank tests of a horizontal-axis turbine

David Lande-Sudall, Sondre Tolleifsen, Kjetil Gravelsæter, Harald Moen and Jan Bartl

Abstract—**Accurate and reliable experimental test data remains a vital part of prototype development for new tidal stream and offshore wind turbines, whereby the numerical models built for verifying device performance and loading need to be validated thoroughly. A test-bed turbine has been developed for this purpose, for use at the MarinLab towing tank in Bergen, Norway. In this paper, a standard rotor geometry with diameter 0.7 m has been used for initial benchmark testing against existing experimental data from similar hydrodynamic test facilities. The rotor blades are 3D printed to enable rapid prototyping of future optimised blade geometries. Inflow speeds at the rotor plane were varied between $U_\infty = 0.4 - 0.8$ m/s, in both zero and 5.5% ambient turbulence intensity. Good agreement on power and thrust coefficients were found across a tip-speed ratio (TSR) range between 0 to 5. Above $TSR = 5$, the turbine gave higher output than existing test data, however, both the blockage ratio and turbulence intensity was higher in this study. Large torque oscillations were observed between the stall and design TSR regions, though in future this behaviour can possibly be dampened by improving the regulation tuning of the dynamometer controller.**

Index Terms—**Experimental tidal turbine, Performance testing, Towing tank, Hydrodynamic test facility.**

I. Introduction

DESPITE numerous limitations in testing at reduced scale, laboratory testing remains an essential step in device design; informing numerical modelling methods and their associated design coefficients which can be tuned and validated against measurements from a controlled laboratory environment. Whether for wind turbine design [1] or tidal stream turbine design [2]–[5], water tank testing has provided valuable data on rotor loading [6] and [7], device wake recovery [8] and [9], and farm/array interactions [10] and [11]. New experimental apparatus nevertheless requires characterising, to assess the facility's accuracy and determine the levels of uncertainty associated with results. No two facilities are identical, with testing procedures differing between them, thus there has been a push to standardise the methodologies used [12], [13]. In order to quantify the effect of hydrodynamic testing facility on model-scale tidal turbine performance, the authors in [14] conducted identical measurements using a standard protocol at three facilities; CNR-INSEAN, IFREMER and the Kelvin Hydrodynamics Laboratory (KHL). Here, differences in time-varying thrust and power were believed to arise from differences in turbulence inflow between recirculating flumes and carriage vibrations in towing tanks. Similarly, [15] and [16] conducted 'Blind test' comparisons for wind turbine aerodynamic performance and wakes. These datasets have been invaluable for informing industry comparisons of numerical modelling [17], [18].

The MarinLab towing tank at the Western Norway University of Applied Sciences was inaugurated in 2016, and has since been used for a range of model testing of floating wind turbines [19], installation vessels [20], and multi-rotor wind turbine systems [21]. Recently, a horizontal-axis turbine test-bed has been designed for use in the facility. In order to assess the suitability of the device and facility for conducting performance tests of future novel rotor geometries, the test-bed platform has been tested with the same rotor geometry as [11], [14], [22], with and without ambient turbulence inflow. In this paper, the results of these initial tests are presented, firstly with a summary of the device design and instrumentation, before introducing the experimental methodology, and subsequently results on tower drag, rotor performance, torque and structural response.

II. Design and manufacture

A test-bed hydrokinetic turbine has been designed and manufactured in-house for use in the MarinLab towing-tank at the Western Norway University of Applied Sciences, Bergen. This facility is a 50 m long tank, with 3.0 × 2.2 m section and is fitted with two towing carriages (master and slave), capable of towing with a maximum velocity of 5.0 m/s and acceleration at 1.2 m/s^2, with 0.001 m accuracy in position. In order to keep blockage effects to a minimum ($< 5\%$), the test-bed dynamometer is designed for use with rotor diameters, $D = 2R$, typically in the range 0.5-0.6 m, for a maximum tip-speed ratio, TSR (Eq.(1)), around 10 at $U_\infty = 1$ m/s inflow velocity. These parameters define the design envelope for the turbine drive-train, with maximum foreseeable thrust, T and torque, Q, in the region of 120 N and 4 Nm, respectively.

$$TSR = \frac{\omega R}{U_\infty} \tag{1}$$

In Equation (1), ω is the rotational speed of the rotor in rad/s.

The test-bed has been heavily inspired from the design and personal discussions with the authors in

This work was supported in part by the Research Council of Norway under grant No. 324388

All authors are with the Western Norway University of Applied Sciences, Inndalsveien 28, Bergen 5063, Norway (e-mail: dla@hvl.no).

S. Tolleifsen is also at the University of Bergen, Department of Physics and Technology, Allégaten 55, 5020 Bergen .

Digital Object Identifier:
https://doi.org/10.36688/ewtec-2023-545

[23]. In their study, the turbine was 1.2 m diameter and bed-supported, with transducers measuring thrust and torque on the rotor and streamwise root bending moment on each blade. However, due to the smaller rotor diameter and hence smaller torque requirements in the MarinLab, a narrower nacelle and corresponding motor/gearbox diameter has been incorporated. The dynamometer consists of a 200 W Maxon EC-i brushless motor (No. 634043) with 12:1 planetary gearbox (No. 223083) providing 15 Nm maximum continuous torque and an EPOS4 50/15 positioning controller (No. 504383) with 4096 step digital encoder (No. 575827). A torque-thrust (*QT*) transducer of 5 Nm and 100 N capacities, with similar design to [24] has been custom-made by Marin, Netherlands. A 480 W Mean Well 48V DC power supply (HEP-480-48A) is used for powering the dynamometer, with any excess power generated being absorbed by a 50 Ω resistor with 200 W rating (RS200). After two design iterations of the aluminium nacelle housing, the final outer diameter around the central tower-nacelle connection boss is 96 mm, with an overall length of 760 mm. Prior to assembly with the dynamometer electronics, a water-tightness test conducted under a compressed air supply, found a leak at the top of the tower-nacelle boss and required a new O-ring groove to be machined. A humidity sensor (DHT11) was subsequently added at the tower-nacelle interface, connected to LabView via an Ardunio microprocessor to provide a warning alarm should the humidity level exceed 60%, indicating possible water ingress.

A. Rotor design

In order to benchmark the test-bed, the well-documented rotor geometry from [11], [14], [22] with diameter, $D = 0.7$ m and NACA 63_3-418 airfoil section is chosen, despite being larger than the diameter range of the design envelope. In order to not exceed the torque capacity from the *QT*-sensor, the inflow speed is limited to $\max\{U_\infty\} = 0.8$ m/s. The foil co-ordinates from [25] are shown in Figure 1 and the chord and twist distribution is identical to those given in [11]. The overall intended design parameters are summarised against those implemented in this benchmark study in Table I.

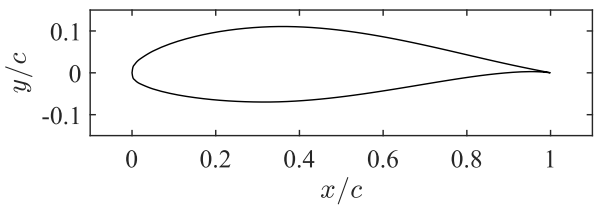

Fig. 1: Airfoil co-ordinates normalised by chord-length, c for the NACA 63_3-418 profile from [25].

To enable rapid prototyping of future model-scale blades, such as those optimised for particular performance requirements e.g. [26], a FlashForge Adventurer 4 [27], 3D printer has been used with ABS plastic at 100% infill to minimise water ingress. The available print volume is limited to $220 \times 200 \times 250$ mm whilst the total blade length is 296 mm, so the inner third of the blade (root) is printed separately to the outer two-thirds of the blade (tip). The two sections are joined with universal water-resistant glue and two M5 threaded rods, to prevent excessive torsion and bending of the blade tip. The minimum trailing edge thickness was defined to 0.2 mm. The three blades took approximately 36 hours to print and were lightly hand-sanded with 600 g/m^2 paper to remove minor surface defects at the leading edge (see inset to Figure 2). The complete assembled turbine is shown in the main image to Figure 2.

TABLE I: Intended design parameters for the test-bed turbine, versus those tested in this benchmark study.

Symbol	Parameter	Design range	Benchmark
U_∞	Inflow speed	0-1 m/s	0.4-0.8 m/s
d	Tower diameter	50 mm	
D	Rotor diameter	500-600 mm	700 mm
D_{nac}	Nacelle diameter	96 mm	
l_{nac}	Nacelle length	760 mm	
Q	Torque rating (sensitivity)	5 Nm (0.006 Nm/V)	
T	Thrust rating (sensitivity)	100 N (0.23 N/V)	

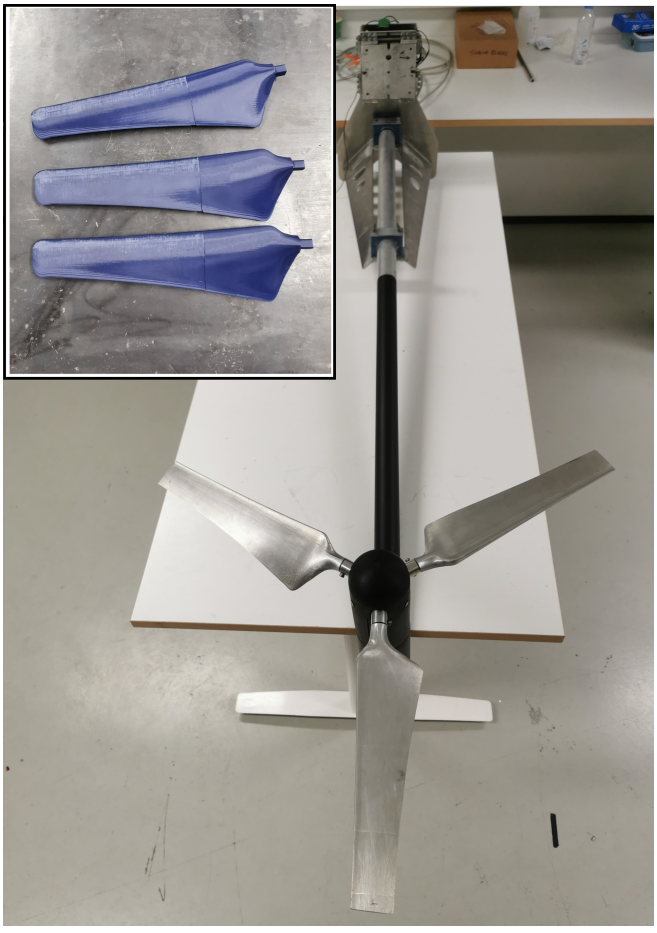

Fig. 2: Complete turbine assembly, mounted with machined aluminium blades and showing load cell attachment to the top of the tower. The image inset shows the 3D printed ABS blades with NACA63_3-418 foil section used in this study.

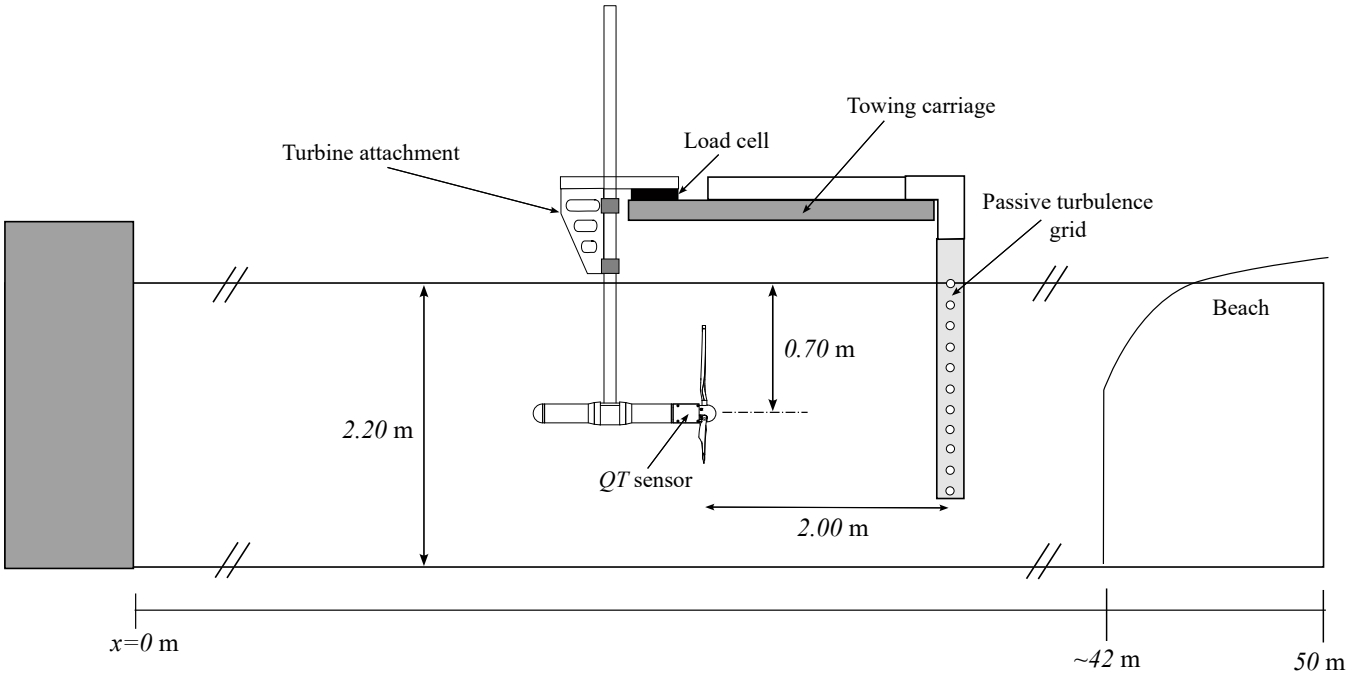

Fig. 3: Schematic diagram (not to scale) of the 50 m long and 3 m wide MarinLab towing tank, showing the turbine attached to the master towing carriage, placement of the tower load cell, torque-thrust transducer and passive turbulence grid.

B. Dynamometer control

Torque and thrust signals from the *QT*-sensor are passed via a 56 mm outer-diameter, 12-wire Senring H1256-12S slip ring, to a National Instruments (NI) 9237 AI Bridge module housed on a NI cDAQ-9184 data acquisition system and recorded into NI LabView at 2000 Hz. The encoder output signal is connected via RS232 communication, which has a minimum refresh rate of approximately 10 ms. Due to further processing time of the encoder signal inside LabView, the encoder is sampled four times with 80 ms intervals, inside the first half of a 0.5 s timed-loop, in order to obtain the time-averaged rotational speed over each 0.5 s interval. Whilst this limits the time-resolution of the rotational speed, this is only a limitation on the collected signal as opposed to the motor controller feedback rate itself, which receives all 4096 pulses per revolution and is controlled with a constant velocity controller. Future improvements will include communication to the motor via a CAN bus interface to allow up to a 1 ms refresh rate.

III. Experimental methodology

The MarinLab towing tank at the Western Norway University of Applied Sciences has a total length of 50.0 m, width of 3.0 m and depth of 2.2 m, with quiescent fluid of nominally 0% turbulence intensity, I.

The test-bed turbine is mounted to the towing carriage, as shown in Figure 3, with a HBM 10 kgf U9C miniature tension-compression load cell measuring the combined tower drag and rotor thrust. Unfortunately, due to a wiring fault from the *QT*-sensor, only the torque could be measured and the rotor-only thrust was not available for this study. Thus all thrust measurements referred to herein are from the load cell at the top of the turbine tower.

A. Grid-generated turbulence

The turbine's performance was tested with both zero ambient turbulence and $I = 5.5\%$ turbulence intensity generated by a passive grid. The grid was mounted at the front of the towing carriage (see Figure 3). The grid has a total submerged cross section of 1.5 m $\times$ 1.4 m, covering about 32% of the towing tank's cross sectional area.

The main dimensions of the grid are sketched in Figure 4(a). It consists of a 50×100 mm rectangular stainless steel frame and an aluminium grid of 14 vertical and 14 horizontal cylindrical tubes. The tubes have a diameter of 20 mm and a centre-to-centre distance of $M = 0.1$ m, resulting in a total grid solidity of σ = 0.36. The ambient velocity behind the grid is reduced with respect to the towing velocity, while ambient turbulence is created. The mean and turbulent flow behind the grid was measured by traversing a *Nortek Vectrino+* Acoustic Doppler Velocimeter (ADV) [28] in streamwise, transverse and vertical directions on an automated traverse. The ADV measures the Doppler frequency shift scattered back from seeding particles distributed in the tank and calculates the three-dimensional velocity vector, (U, V, W), at 200 Hz sampling frequency from a small cylindrical measurement volume of length 15 mm. More details about ADV flow measurements in the MarinLab towing tank can be found in [21].

The flow characteristics behind the grid were measured at a towing speed of $U_\infty = 0.4$ m/s, with turbulence intensity calculated according to Equation 2. At the location of the turbine rotor, 2.0 m downstream of the grid, the velocity was reduced by about 14% from the towing speed, and found to vary by not more than 2% over the cross sectional area covered by the grid. As depicted in Figure 4(b), the velocity reduction

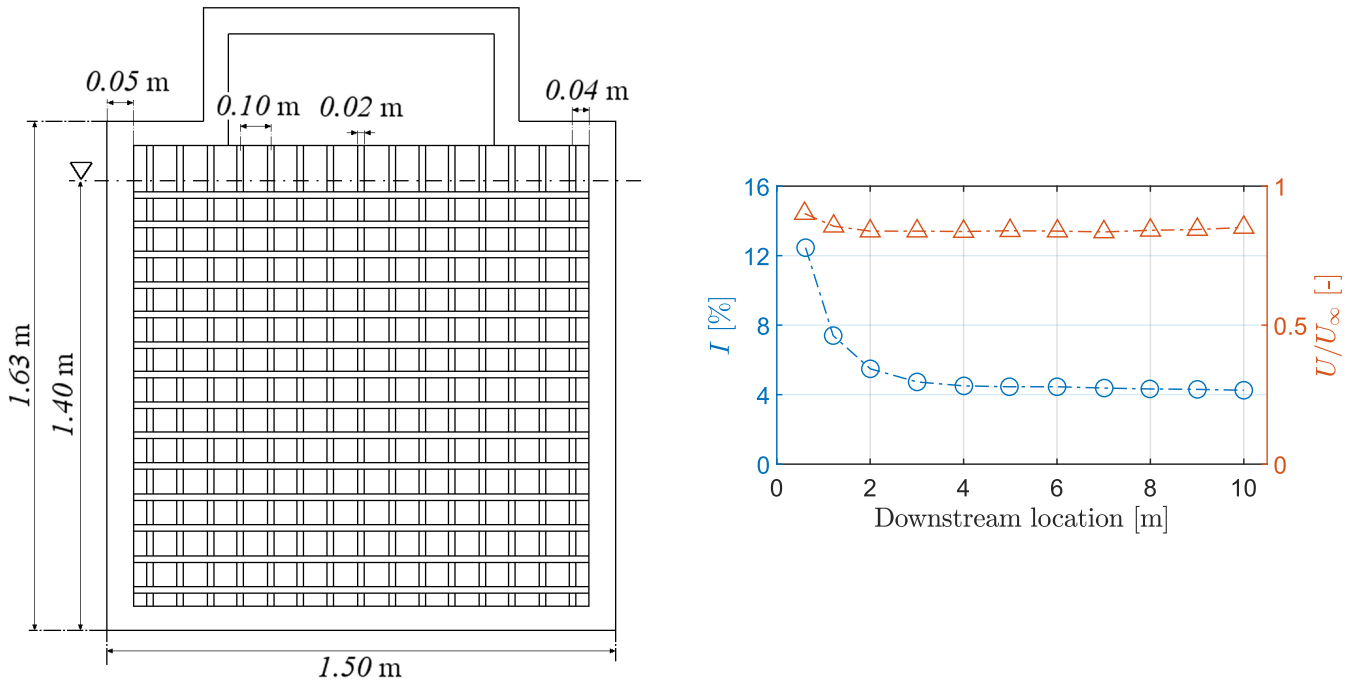

Fig. 4: (a) Front view of the passive turbulence grid, and (b) Variation in turbulence intensity, I [%] (blue) and velocity reduction U_∞/U_{tow} [-] (red) with downstream locations measured along the centreline of the turbulence grid.

tends to an asymptote from approximately 2 m to 10 m downstream. Along the downstream centreline of the grid, the measured turbulence intensity decays from over $I_{0.4\text{m}}$ = 12% at 0.4 m downstream, to about $I_{10\text{m}}$ = 4% by 10 m. At the location of the turbine rotor an ambient turbulence of $I_{2\text{m}}$ = 5.5% was created. Additional measurements in crosswise and vertical directions confirmed homogeneous turbulence levels within $\pm 0.5\%$, with the exception of a local increase of $+2\%$ behind the frame holding the grid.

$$I = \sqrt{\frac{\frac{1}{3}(u^2 + v^2 + w^2)}{\overline{U}^2 + \overline{V}^2 + \overline{W}^2}} \tag{2}$$

In Equation 2, bar-notation represents the mean part, and lower-case characters the fluctuating part.

B. Test-cases

A total of three inlet velocities at the rotor plane, $U_\infty = 0.4$, 0.6 and 0.8 m/s are tested, with and without passive turbulence generation. Additionally, the tower-only drag was measured for each towing speed in zero ambient turbulence. All test-cases are summarised in Table II.

TABLE II: Test-cases used in this study. U_{tow} is the carriage towing speed and U_∞ is the velocity observed at the rotor-plane without the turbine present.

U_{tow}, m/s	U_∞, m/s	I, %	Tower-only	Rotor & tower
0.4	0.4	0	✓	✓
0.6	0.6	0	✓	✓
0.8	0.8	0	✓	✓
0.45	0.4	5.5	-	✓
0.68	0.6	5.5	-	✓
0.90	0.8	5.5	-	✓

Due to a finite tank length, all tests were specified with a maximum run distance of 37 m, with acceleration/deceleration of 0.3 m/s^2, giving a total acquisition duration varying between approximately 45-90 s. After cropping the inertial ends from each run, the typical sample duration was between 25-60 s. Due to time limitations, repeat measurements were only conducted in the regions of TSR 2.5-3.5 for all cases and for cases where anomalous time-averages were first obtained. Two repeat measurements were taken for every TSR point in the $U_\infty = 0.6$ m/s case with turbulence. All time-averaged values presented here are an ensemble average of all available repetitions.

IV. Results

Results for the tower-drag are first presented, before discussing performance curves, time-varying torque and structural response.

A. Tower-drag

Since the thrust measurements from the *QT*-sensor were not available, thrust could only be measured from the tower load cell. To establish the contribution of the tower drag towards the net thrust, the tower-only drag (i.e. without nacelle) and tower-with-nacelle drag were measured for the case of zero ambient turbulence and no rotor, with towing speeds ranging from 0.2 to 1.0 m/s, as presented in Figure 5. Quadratic least-squares fit lines to each data set show good agreement. Compared to the cases with nacelle, the larger standard deviations found at low speeds for the tower-only cases are expected to be due to the overall lighter mass of the tower-only being more sensitive to carriage vibrations. For $U_\infty = 0.8$ and 1.0 m/s, the standard deviation of the tower-with-nacelle case grows, which was visibly observed as the onset of some tower vibrations. These

vibrations were possibly vortex-induced, presumably due to the extra mass of the nacelle providing a lower natural frequency which then may approach the vortex shedding frequency for the tower with nacelle. More frequency analysis is considered for the cases with the rotor in Section IV-D.

In dimensionless form, the mean drag coefficient for the tower-only is $C_{D,twr} = 1.20$ and tower with nacelle is $C_{D,twr+nacelle} = 1.11$, where the referenced projected areas are that of the tower-only and tower-with-nacelle, respectively. Since results in [14] are presented with tower drag included, and due to the uncertainty in methods of trying to isolate the rotor thrust, all further results on thrust in this paper are presented with tower-drag included.

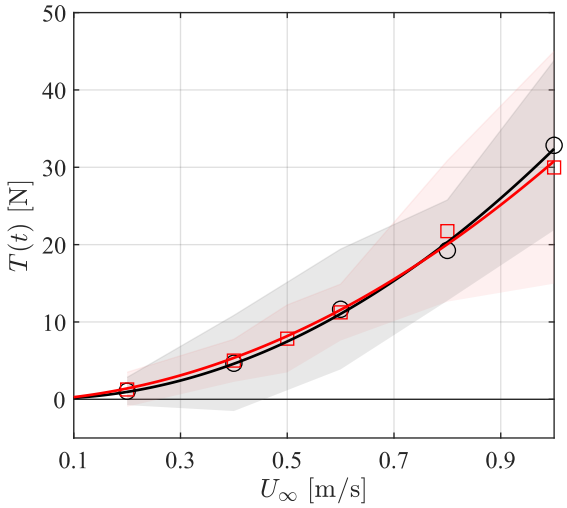

Fig. 5: Time-averaged drag force for the tower-only (black) and tower with nacelle (red) with zero ambient turbulence. Shaded areas represent $\pm\sigma$ standard deviation, and solid lines are quadratic curves least-squares fit to the data and through the (0,0) origin.

B. Rotor power coefficient, C_P and thrust coefficient, C_T

In this section, results of the rotor performance and thrust coefficients, C_P and C_T are presented, where we follow the standard definitions in Equation (3) and Equation (4), respectively:

$$C_P = \frac{8\omega Q}{\rho\pi D^2 U_\infty^3} \tag{3}$$

$$C_T = \frac{8T}{\rho\pi D^2 U_\infty^2} \tag{4}$$

where ρ=1000 kg/m^3 is taken as the density of freshwater.

Data from KHL and CNR-INSEAN towing tanks [14] are used for comparison. The global blockage ratio of rotor swept-area to tank cross-section is $B = 5.8$ % in MarinLab. This is larger than the 3.3% and 1.2% blockage ratios of KHL and CNR-INSEAN, respectively. Whilst various methods of blockage correction exist [29], [30], we present the results without any correction applied to allow direct comparison to non-corrected results from [14] and to avoid any ambiguity of the post-processing..

Figure 6 (a) shows the C_P and $C_T(TSR)$ curves without turbulence, compared to curves from KHL and CNR-INSEAN towing tanks [14] with $U_\infty = 0.8$ m/s. For the MarinLab turbine, at $U_\infty = 0.4$ m/s, there is a significant reduction in both C_P and C_T. As reported in [14], low-Reynolds number effects are likely generated, with unstable laminar separation bubbles forming for such low towing speeds [31], where the chord-based Reynolds number at $0.7R$ is only $Re_c \sim 50$k, for TSR=3.5. Such effects act to destroy the lift generated by the foil and thus the local torque and power. For $U_\infty = 0.6$ m/s, this drop in C_P is not observed and very close agreement to [14] is found for TSR values from 0 to 5. For $TSR > 5$, the MarinLab test-bed generates higher values of C_P. A similar result, but to a greater extent, is also visible for the $U_\infty = 0.8$ m/s case. This could be due to possible local twisting of the 3D printed blades, where even small angles ($< -5°$) would benefit C_P, although this was not visually confirmed. Alternatively, since the measurement points have not been corrected for blockage, it could be a result of this, where blockage would tend to have a greater effect at higher TSRs. Lastly, the carriage speed was not measured directly, and whilst previous ADV measurements in [21] have shown good agreement with the target carriage speed, power is particularly sensitive to small discrepancies.

In general, mean C_T is slightly lower than for the KHL and CNR-INSEAN results, however, the submersion depth used in MarinLab was only 0.7 m compared to 1.0 m in [14], which would account for much of this discrepancy. 0.7 m depth was chosen here due to the need to centralise the turbine behind the available turbulence grid (Fig. 4). The standard deviation in thrust coefficient is generally of a similar, low magnitude for all towing speeds. However, between $2 < TSR < 3$ the standard deviation increases significantly. In Section IV-D it is discussed if this oscillation is related to the turbine's structural response. Alternatively, this region is in the transition from where much of the blade is predominantly in stall to it then generating maximum lift at slightly higher TSR. It may also be related to the possibility of a critical Reynolds number being reached for the local airfoil section, where the Reynolds number is affected by both towing and rotational speeds. This TSR region is thus very unstable and hence leads to a large temporal oscillations in thrust. Further discussion with regards to torque is found in Section IV-C.

In Figure 6(b) with turbulence inflow, the $C_P(TSR)$ curves from $U_\infty = 0.4$ to 0.8 m/s collapse on top of each other. Ambient turbulence will hinder the formation of laminar separation bubbles, hence improving the performance for $U_\infty = 0.4$ m/s compared to no turbulence. This contrasts with the results in [11] for $U_\infty = 0.4$ m/s and $I = 3\%$, where there was still a significant drop in C_P. However, in MarinLab the turbulence intensity was greater, at $I = 5.5\%$ and [11] also reported for $I = 15\%$ that the C_P curves increased compared to $I = 3\%$ for $U_\infty = 0.4$ m/s. In terms of thrust, C_T for $U_\infty = 0.8$ m/s is consistently lower for $TSR > 2.5$, which may be an indicator of some coning of the 3D printed rotor for high towing speeds.

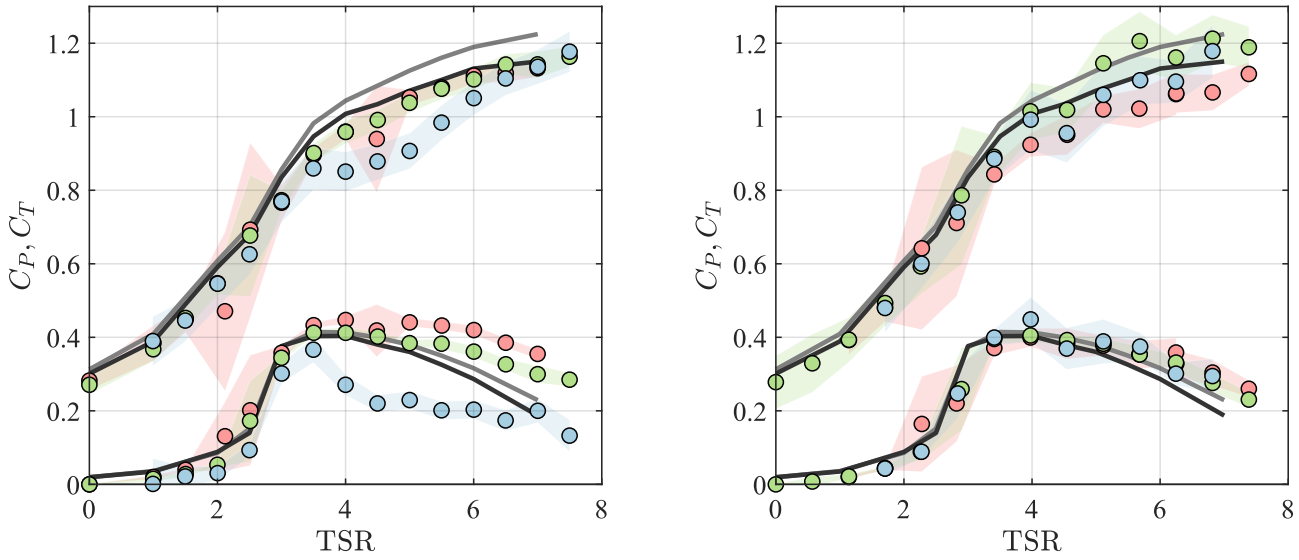

Fig. 6: C_P and C_T versus tip-speed ratio, TSR, for (a) zero ambient turbulence and (b) 5.5% ambient turbulence intensity. Mean (○) and standard deviation $\pm\sigma$ (shaded areas) for $U_\infty = 0.4$ m/s (blue), $U_\infty = 0.6$ m/s (green) and $U_\infty = 0.8$ m/s (red), along with reported values from KHL (—) and CNR-INSEAN (—) at $U_\infty = 0.8$ m/s from [14].

C. Rotor torque, Q

With the benchmark turbine diameter being 0.1 m larger than the maximum 0.6 m intended for the *QT*-sensor rating, it was necessary to pay close attention to the torque magnitudes, especially for the highest tow-speed with turbulence generation.

Figure 7 shows a sample time-series of $Q(t)$ for $U_\infty = 0.6$ m/s and $TSR = 2.5$ and 3.5, with the latter representing the design TSR of the rotor. Evident, is a large difference in mean rotor torque for $TSR = 2.5$ compared to 3.5, which is expected given the transition from the stall-region of the TSR curve to optimal performance. However, of more significance are the large oscillations in torque for $TSR = 2.5$; cycling between approximately -1 Nm to +3.5 Nm. From visual inspection, this appeared as the rotor turning before abruptly braking to nearly zero rotational speed, before continuing to rotate again. The cause of this is not immediately apparent. As mentioned, $TSR = 2.5$ is at the transition between the rotor operating predominantly in stall, to generating maximum power output at $TSR = 3.5$. From a mechanical perspective, at $U_\infty \geq 0.6$ m/s, $TSR = 3.5$ is where the turbine transitions from requiring a net power input, to generating a net power output, which is passively diverted into the electrical resistor. However, torque oscillations were still noted for $U_\infty = 0.4$ m/s, when there was no net power output. Given that the torque oscillations are well within the maximum continuous torque rating of the motor gearbox, and within the *QT*-sensor capacity, it seems to be a product of the motor controller not being able to respond adequately to the large fluctuations in torque which arise in this transition region. Nevertheless, the mean C_P and C_T values still match those of [14] well. Thus, as long as the turbine is studied outside of this transition region, it still provides the anticipated load characteristics.

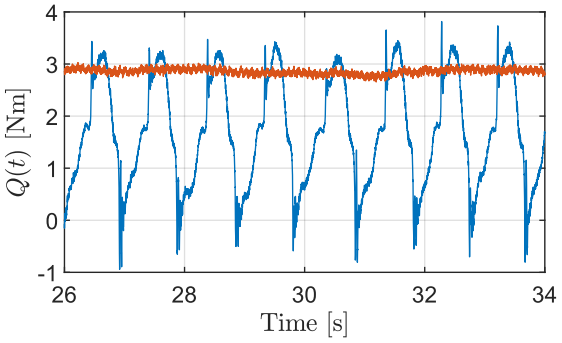

Fig. 7: Sample time-series measurements of torque, $Q(t)$ for TSR=2.5 (blue) and TSR=3.5 (red).

D. Structural response

Although the turbine attachment (Fig. 3) features a large support bracket to increase bending stiffness, clear vibrations of the tower were still observed for some of the test-cases. To investigate this further we follow Welch's method [32], to obtain the Power Spectral Density (PSD) for $U_\infty = 0.6$ m/s at $TSR = 2.5$ and 3.5 in Figure 8 using four windows, with 50% overlap and a Hann window to remove any spectral artefacts arising from having an otherwise discontinuous windowed signal. The first blade passing frequency, 1P, is identified for each TSR case. For $TSR = 2.5$, there is a clear peak in the signal at 1.09 Hz, which is greater than the expected 1P frequency (0.68 Hz). However,

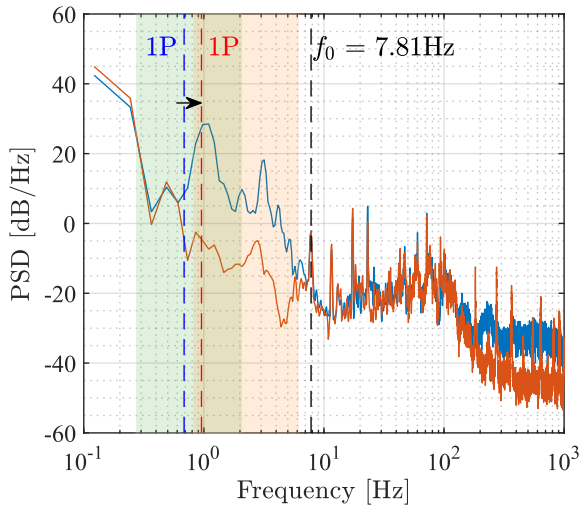

Fig. 8: Power-spectral density of the tower thrust response, for $TSR = 2.5$ (blue) and $TSR = 3.5$ (red). Showing the tower structural eigenfrequency, f_0 and range of 1P (green shaded) and corresponding 3P (orange shaded) blade-passing frequencies between $1 < TSR < 7.5$.

as discussed for Figure 7 for this TSR case, the rotor was oscillating between rotation and braked, resulting in significant oscillations in torque which necessarily impacts thrust. Given that during each oscillation the rotor is momentarily braked, then when the turbine rotates again, the motor controller requires the rotational speed to be greater than the target 0.68 Hz in order to maintain a steady average. Unfortunately due to time limitations and a concern of overloading the QT-sensor from the large inertia of the blades whilst mounted to the hub, the motor's PID controller was not tuned to provide slower feedback, which could potentially help dampen these severe oscillations.

In contrast, $TSR = 3.5$ has a less significant peak near the 1P frequency, which aligns with the visual observations of minimal tower vibrations occurring for this run, and indeed is indicative of all cases outside of $2 \leq TSR \leq 3$. Figure 8 also highlights the ranges expected for 1P and 3P frequencies for the tested TSR range. In both $TSR = 2.5$ and 3.5, the 3P frequency is evident as the largest peak in the shaded (orange) region. The natural frequency of the tower, f_0 is identified with a common peak in both signals at 7.81 Hz. Given that this frequency is outside of the 1P and 3P ranges, then the tower is a stiff-stiff construction and will not be excited to resonance. However, should for example heavier aluminium blades be used in future with this rotor diameter, there is a risk that the tower natural frequency will reduce, possibly to inside the 3P operating range.

V. Conclusion and Future Work

A test-bed horizontal-axis turbine has been designed and tested at the Western Norway University of Applied Sciences, MarinLab towing tank in Bergen, Norway. The turbine is instrumented with thrust and torque sensors and an encoder to resolve turbine power. A NACA 63_3-418 foil was used for the rotor geometry to be directly comparable to tests in [11], [14], [22] for benchmarking purposes. For tip-speed ratios, $TSR < 5.5$, the turbine gives comparable mean performance (C_P and C_T) to [14] with $U_\infty = 0.4 - 0.8$ m/s. However, large oscillations in torque around the stall transition at $TSR = 2.5$ were observed. Future tests will investigate tuning the motor controller to provide slower feedback and maintain better speed regulation in this region. Also, low Reynolds number effects were apparent for the case of $U_\infty = 0.4$ m/s without turbulence and so the minimum tow-speed for this rotor should not be less than $U_\infty = 0.6$ m/s in order to avoid this. Use of a passive turbulence grid allowed testing with turbulence intensity of 5.5%. Here it was found that low-Reynolds number effects vanished at $U_\infty = 0.4$ m/s, and there was closer agreement on C_P for all towing speeds, whilst C_T was marginally lower for $U_\infty = 0.8$ m/s. A second turbulence grid available in the lab, with 50 mm cylindrical tubes and centre-centre spacing of $M = 0.25$ m can enable testing with turbulence intensities of $> 6\%$ in future.

A method of rapid prototyping the turbine blades using a 3D printer has proven effective, especially around the design TSR rating, and future tests with Kriging-optimised rotors [26], representing both model scale tidal stream turbines and offshore wind turbines, are planned. A LaVision Shake-the-Box [33] tomographic particle tracking velocimetry system is also available in MarinLab and future testing will make use of this for providing time-resolved wake measurements downstream of the turbine, potentially helping to isolate some sources of performance discrepancies observed here, e.g. at $TSR > 5$, where there was uncertainty on whether the blades were coning or if this was due to blockage. Finally, the QT-sensor is equipped with additional wiring through to the hub, to allow blade-root bending to be measured in future, along with re-establishing the hub thrust signal.

VI. Acknowledgements

The authors are thankful for constructive discussions with Grégory Payne and Robert Larsson on design considerations for the turbine, Nafez Ardestani and Gloria Stenfelt for lab assistance, and to BSc students Bendik Weltzien, Hans Joakim Jakobsen and Nikolai Arntzen for the CAD drawings of the final design iteration. Thank you also to Carola Buness for performing flow measurements behind the passive grid. This work has been partly supported by the Research Council of Norway, grant No. 324388).

References

[1] V. L. Okulov, R. Mikkelsen, J. N. Sørensen, and I. V. Naumov, "Power Properties of Two Interacting Wind Turbine Rotors," vol. 139, no. September, pp. 1–6, 2017.

[2] A. Bahaj, W. Batten, and G. McCann, "Experimental verifications of numerical predictions for the hydrodynamic performance of horizontal axis marine current turbines," *Renewable Energy*, vol. 32, no. 15, pp. 2479–2490, Dec. 2007. [Online]. Available: https://linkinghub.elsevier.com/retrieve/pii/S0960148107002996

[3] L. Myers and A. Bahaj, "Near wake properties of horizontal axis marine current turbines," *8th European Wave and Tidal Energy Conference*, pp. 558–565, 2009.

[4] J. McNaughton, B. Cao, S. Ettema, F. Zilic De Arcos, C. Vogel, and R. Willden, "Experimental testing of the performance and interference effects of a cross-stream array of tidal turbines," in *Developments in Renewable Energies Offshore*, 1st ed., C. Guedes Soares, Ed. CRC Press, Oct. 2020, pp. 563–570. [Online]. Available: https://www.taylorfrancis.com/books/9781000318739/chapters/10.1201/9781003134572-64

[5] G. S. Payne, T. Stallard, R. Martinez, and T. Bruce, "Variation of loads on a three-bladed horizontal axis tidal turbine with frequency and blade position," *Journal of Fluids and Structures*, vol. 83, pp. 156–170, Nov. 2018. [Online]. Available: https://www.sciencedirect.com/science/article/pii/S0889974617306734

[6] T. Blackmore, L. E. Myers, and A. S. Bahaj, "Effects of turbulence on tidal turbines: Implications to performance, blade loads, and condition monitoring," *International Journal of Marine Energy*, vol. 14, pp. 1–26, 2016, publisher: Elsevier Ltd. [Online]. Available: http://dx.doi.org/10.1016/j.ijome.2016.04.017

[7] R. Martinez, B. Gaurier, S. Ordonez-Sanchez, J.-v. Facq, G. Germain, C. Johnstone, I. Santic, F. Salvatore, T. Davey, C. Old, and B. G. Sellar, "Tidal Energy Round Robin Tests: A Comparison of Flow Measurements and Turbine Loading," *Journal of Marine Science and Engineering*, vol. 9, no. 4, p. 425, 2021. [Online]. Available: https://www.mdpi.com/2077-1312/9/4/425

[8] T. Stallard, T. Feng, and P. Stansby, "Experimental study of the mean wake of a tidal stream rotor in a shallow turbulent flow," *Journal of Fluids and Structures*, vol. 54, pp. 235–246, Apr. 2014, publisher: Elsevier. [Online]. Available: http://linkinghub.elsevier.com/retrieve/pii/S0889974614002485

[9] D. Lande-Sudall, T. Stallard, and P. Stansby, "Experimental Study of the Wakes due to Tidal Rotors and a Shared Cylindrical Support," in *Proceedings of 12th European Wave and Tidal Energy Conference, Cork, Ireland*, 2017.

[10] T. Stallard, R. Collings, T. Feng, and J. Whelan, "Interactions between tidal turbine wakes: experimental study of a group of three-bladed rotors." *Philosophical transactions. Series A, Mathematical, physical, and engineering sciences*, vol. 371, no. 1985, p. 20120159, Feb. 2013. [Online]. Available: http://www.ncbi.nlm.nih.gov/pubmed/23319702

[11] P. Mycek, B. Gaurier, G. Germain, G. Pinon, and E. Rivoalen, "Numerical and experimental study of the interaction between two marine current turbines," *International Journal of Marine Energy*, vol. 1, pp. 70–83, Apr. 2013. [Online]. Available: https://www.sciencedirect.com/science/article/pii/S2214166913000088

[12] D. Ingram, G. Smith, C. Bittencourt-Ferreira, and H. Smith, "Protocols for the Equitable Assessment of Marine Energy Converters," University of Edinburgh, Tech. Rep., 2011. [Online]. Available: https://www.pure.ed.ac.uk/ws/portalfiles/portal/1726320/book1.pdf

[13] ITTC, "ITTC – Recommended Procedures and Guidelines: Model Tests for Current Turbines 7.5-02 07-03.9," ITTC, Tech. Rep., 2021. [Online]. Available: https://www.ittc.info/media/9749/75-02-07-039.pdf

[14] B. Gaurier, G. Germain, J. V. Facq, C. M. Johnstone, A. D. Grant, and A. H. Day, "Tidal energy " Round Robin " tests comparisons between towing tank and circulating tank results," *International Journal of Marine Energy*, vol. 12, no. December, pp. 87–109, 2015.

[15] J. Bartl and L. Sætran, "Blind test comparison of the performance and wake flow between two in-line wind turbines exposed to different turbulent inflow conditions," *Wind Energy Science*, vol. 2, no. 1, pp. 55–76, Feb. 2017. [Online]. Available: https://wes.copernicus.org/articles/2/55/2017/

[16] F. Mühle, J. Schottler, J. Bartl, R. Futrzynski, S. Evans, L. Bernini, P. Schito, M. Draper, A. Guggeri, E. Kleusberg, D. S. Henningson, M. Hölling, J. Peinke, M. S. Adaramola, and L. Sætran, "Blind test comparison on the wake behind a yawed wind turbine," *Wind Energy Science*, vol. 3, no. 2, pp. 883–903, Nov. 2018, publisher: Copernicus GmbH. [Online]. Available: https://wes.copernicus.org/articles/3/883/2018/

[17] F. Pierella, P.- Krogstad, and L. Sætran, "Blind Test 2 calculations for two in-line model wind turbines where the downstream turbine operates at various rotational speeds," *Renewable Energy*, vol. 70, pp. 62–77, Oct. 2014. [Online]. Available: https://www.sciencedirect.com/science/article/pii/S0960148114001815

[18] P.- Krogstad and L. Sætran, "Wind turbine wake interactions; results from blind tests," *Journal of Physics: Conference Series*, vol. 625, p. 012043, Jun. 2015. [Online]. Available: https://iopscience.iop.org/article/10.1088/1742-6596/625/1/012043

[19] A. M. T. Ripe, "An Assessment of Extreme Mooring Loads for Floating Offshore Wind Structures Using Conditional Waves," Ph.D. dissertation, University of Bergen, Department of Physics and Technology, Aug. 2022. [Online]. Available: https://bora.uib.no/bora-xmlui/bitstream/handle/11250/3014612/HTEK399_final.pdf?sequence=1&isAllowed=y

[20] D. R. Lande-Sudall, T. S. Høyven, K. Herfjord, and T. C. Thuestad, "Wave-induced collision loads and moments between a spar-buoy floating wind turbine and an installation vessel," *Journal of Physics: Conference Series*, vol. 1669, no. 1, 2020.

[21] J. Bartl, C. H. Aasnæs, J. R. Bjørnsen, G. Stenfelt, and D. Lande-Sudall, "Lab-scale measurements of wind farm blockage effects," *Journal of Physics: Conference Series*, vol. 2362, no. 1, p. 012004, Nov. 2022. [Online]. Available: https://iopscience.iop.org/article/10.1088/1742-6596/2362/1/012004

[22] P. Mycek, B. Gaurier, G. Germain, G. Pinon, and E. Rivoalen, "Experimental study of the turbulence intensity effects on marine current turbines behaviour. Part I: One single turbine," *Renewable Energy*, vol. 66, pp. 729–746, 2014, publisher: Elsevier Ltd ISBN: 0960-1481. [Online]. Available: http://dx.doi.org/10.1016/j.renene.2013.12.036

[23] G. S. Payne, T. Stallard, and R. Martinez, "Design and manufacture of a bed supported tidal turbine model for blade and shaft load measurement in turbulent flow and waves," *Renewable Energy*, vol. 107, pp. 312–326, 2017.

[24] J. Dang, J. Brouwer, R. Bosman, and C. Pouw, "Quasi-Steady Two-Quadrant Open Water Tests for the Wageningen Propeller C - and D -Series," Gothenburg, Sweden, Aug. 2012, pp. 26–31.

[25] I. Abbott, H., *Theory of Wind Sections - Including a Summary of Airfoil Data*. New York: Dover Publications Inc., 1959.

[26] T. H. Hansen and F. Mühle, "Winglet optimization for a model-scale wind turbine," *Wind Energy*, vol. 21, no. 8, pp. 634–649, 2018, _eprint: https://onlinelibrary.wiley.com/doi/pdf/10.1002/we.2183. [Online]. Available: https://onlinelibrary.wiley.com/doi/abs/10.1002/we.2183

[27] FLASHFORGE, "FLASHFORGE 3D Printer Adventurer 4 Series User Guide," 2021.

[28] Nortek AS, "Comprehensive Manual," NORTEK AS, Tech. Rep., Nov. 2015.

[29] A. S. Bahaj, A. F. Molland, J. R. Chaplin, and W. M. J. Batten, "Power and thrust measurements of marine current turbines under various hydrodynamic flow conditions in a cavitation tunnel and a towing tank," *Renewable Energy*, vol. 32, pp. 407–426, 2007.

[30] G. T. Houlsby and S. Draper, "Application of Linear Momentum Actuator Disc Theory to Open Channel Flow by," University of Oxford, Tech. Rep. OUEL 2296/08, 2008.

[31] M. Drela, *Flight vehicle aerodynamics*. Cambridge (Mass.): MIT press, 2014.

[32] P. D. Welch, "The Use of Fast Fourier Transform for the Estimation of Power Spectra: A Method Based on Time Averaging Over Short, Modified Periodograms," *IEEE Trans. Audio and Electroacoust.*, vol. AU-15, pp. 70–73, 1967.

[33] Y. J. Jeon, "4D Flow Field Reconstruction From Particle Tracks By Vic+ With Additional Constraints and Multigrid Approximation," *BRISK Binary Robust Invariant Scalable Keypoints*, pp. 12–19, 2018, iSBN: 8610828378018. [Online]. Available: https://doi.org/10.3929/ethz-a-010025751